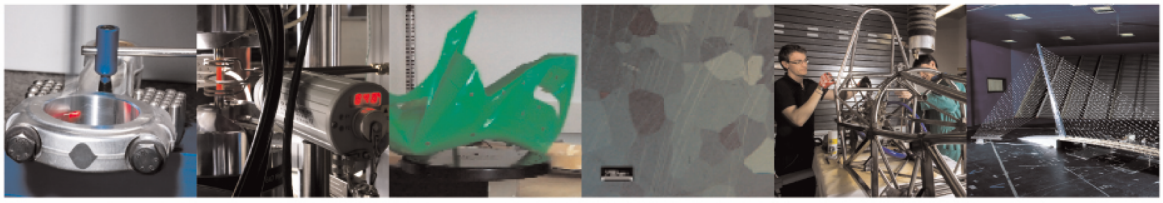

Uncovering the toughening mechanisms of bonded joints through tailored CFRP layup

R.A.A. Lima, R. Tao, A. Bernasconi, M. Carboni, N. Carrere, S. Teixeira de Freitas

This is a post-peer-review, pre-copyedit version of an article published in Composites Part B. The final authenticated version is available online at: https://doi.org/10.1016/j.compositesb.2023.110853

DIPARTIMENTO DI MECCANICA ■ POLITECNICO DI MILANO
via G. La Masa, 1 ■ 20156 Milano ■ EMAIL (PEC): pecmecc@cert.polimi.it
http://www.mecc.polimi.it
Rev. 0

Uncovering the Toughening Mechanisms of Bonded Joints through Tailored CFRP Layup

R. A. A. Lima [a,b], R. Tao [b], A. Bernasconi [a], M. Carboni [a], N. Carrere [c], S. Teixeira de Freitas [b*]

[a] Department of Mechanical Engineering, Politecnico di Milano – Milan, Italy

[b] Faculty of Aerospace Engineering, Delft University of Technology – Delft, Netherlands

[c] ENSTA Bretagne, UMR CNRS 6027, IRDL, F-29200 – Brest, France

Abstract

Aiming to increase damage tolerance of adhesively bonded joints, this work explores the influence of CFRP layup of the adherends on the crack onset and crack propagation of composite bonded joints under mode I loading. Quasi-static double Cantilever Beam tests were performed using four different CFRP layups bonded with two adhesives. Parallel to the experimental program, finite element analyses were performed to aid in understanding and identifying the various damage mechanisms in each specimen type. The results show that the CFRP layup and adhesive fracture toughness significantly influence the joint fracture phenomena at crack onset and further crack propagation. An increase in the joint's mode I fracture toughness at crack onset was observed when a crack compertition was triggered between the crack propagation within the bondline and within the composite's layers. During crack propagation, the fracture toughness of the joint increases at crack deflections between the different plies of the CFRP layup until reaching the 0 degrees ply, where sudden delamination occurs. It is shown that tailoring CFRP layup is a promising toughening method that can increase up to 97% the fracture toughness of the joint when compared to pure cohesive failure.

Keywords: tailored CFRP layup, fracture toughness, bonded joints; toughening mechanisms.

* Corresponding author: e-mail: S.TeixeiraDeFreitas@tudelft.nl (S. Teixeira de Freitas).

1 Introduction

In recent years, global action has increased to reduce CO_2 emissions and improve sustainability in different industrial fields, and the aeronautical field is not an exception. New solutions are being studied to extend the aircraft's operational life and recycle structural components [1]–[3]. Moreover, advanced materials such as newly engineered metal alloys and Carbon Fibre Reinforced Polymers (CFRP) have been steadily used to produce lightweight structures and reduce fuel consumption [2].

In order to achieve efficient light-weight structures, the assembly of multi-material and composites components in primary structures is still a key challenge. Adhesive bonding has advantages, such as the neglectable negative impact on the substrate's mechanical properties, uniform stress distribution, and great design flexibility [2], [4]. Nevertheless, secondary bonding of primary structures is not certified. Adhesive bonding presents limited resistance to crack growth which poses the risk of sudden failure (specially in aggressive environments) [5]–[7]. In addition, it remains a challenge to detect interfacial failure caused by weak bonds using the current Non-Destructive Techniques (NDT) and Structural Health Monitoring (SHM) methods [4], [8]–[10]. Therefore, "backup solutions" such as rivets and bolts have been currently implemented to avoid catastrophic failure in safety-critical applications [11]–[13].

A solution to overcome these limitations and improve the adhesively bonded joint's safety and reliability during their operational life in critical load-bearing applications is to improve the joint's resistance to crack growth, i.e., its fracture toughness. Several methods are proposed in the literature to increase the fracture toughness of composite adhesively bonded joints. Some of these toughening mechanisms are described below:

- Interfacial adhesion patterning over the substrate's surface – is an extrinsic toughening method based on the intentional modification of the interfacial adhesion properties by applying different surface treatments such as pulsed laser irradiation, sandblasting, U.V. radiation and plasma [3], [14], [15] that can trigger bridging mechanisms within the adhesive layer, or by introducing non-sticky Teflon films [16] to tailor sacrificial cracks within the bondline;
- Improvement of the adhesive's mechanical properties – is an intrinsic method based on modifications of the adhesive material by adding micro/nanoparticles (i.e. Carbon Nano Tubes – CNT and Polyhedral-Oligomeric-Sil-Sesquioxanes - POSS) [17]–[22]. These

can either be applied in the complete bondline or in specific regions of the adhesive layer (graded adhesive joints) to architect different mechanical properties throughout the adhesive's length [23];

- Introduction of crack stoppers within the adhesive layer – such as using Z-pinning [7], substrate corrugation, exposing fibres [24], and embedment of woven mats [25] to arrest the crack propagation; or adding 'stop holes' ahead of growing crack to reduce the stress singularities in its tip and further delay the crack growth.

Limited research is found on how the composite substrate layup can affect fracture toughness. For pure composite laminates without material bondline, the effects of different interface ply orientations on the crack paths were intensively investigated in previous work [28]–[30]. However, the contributions of laminates' thickness or local orientation in adhesive joints are limited in the literature [11], [31]–[33].

Kupski et al. [11]. used different composite ply thicknesses in bonded SLJ and concluded that thinner composite plies in the substrates showed multiple transverse matrix cracks, leading to a crack deflection from the bondline to the laminates. This resulted in an increase in the energy dissipation and in the load at the crack onset (initiation). The ply orientation also played a significant role in increasing joint failure strength [31]–[33], and it could enhance the joint's fracture toughness associated with the co-occurrence of many damage mechanisms, such as crack branching and deflection [33].

Nevertheless, there is no agreement on which fracture mechanisms can trigger toughening when using composite layup tailoring, nor the role of adhesive toughness in this phenomenon.

This work aims to analyse how CFRP layup can trigger toughening mechanism of adhesively bonded joints and how the adhesive fracture toughness plays a role on the possible enhancement of the joint's fracture toughness both at crack onset and further crack propagation.

2 Materials and methods

2.1 Specimens manufacturing

The unidirectional carbon fibre prepregs Hexply 8552 – AS4 toughened epoxy resin (Hexcel Composites, Cambridge, UK) was used as a substrate material to produce the DCB specimens. Table 1 lists its main mechanical properties.

Table 1: Materials properties of Hexply 8552 – AS4 [34].

Longitudinal tensile strength	X_T	2207 MPa
Longitudinal compressive strength	X_C	1531 MPa
Transverse tensile strength	Y_T	81 MPa
Longitudinal tensile modulus	E_{11T}	141 GPa
Transverse tensile modulus	$E_{22T} = E_{33T}$	10 GPa
In-plane shear modulus	$G_{12} = G_{13}$	5.2 GPa
Transverse shear modulus	$G_{23} = E_{33T}/(2(1+\nu_{23}))$	3.33 GPa
In-plane shear strength	$S_{12} = S_{13}$	114 GPa
In-plane Poisson ratio	$\nu_{12} = \nu_{13}$	0.27
Transverse Poisson ratio	ν_{23}	0.5

Aiming to study the influence of the laminate's staking sequence on the join's fracture toughness, five different layups were manufactured: $[0]_8$, $[0/90_2/0]_S$, $[90/0_2/90]_S$, $[90/45/-45/0]_S$ and $[90/60/90/-60/0]_S$. Table 2 lists the laminate's longitudinal bending stiffness determined through the flexural engineering constant of the laminate (Eq. 01) based on the classical laminate theory..

$$E_x^f = \frac{12}{D_{11}^* t^3} \qquad \text{Eq. 01}$$

In Equation 01, D_{11}^* represents the value of the first row and column of the inverse bending stiffness matrix, and t (the total thickness of the laminate) is defined by the number of plies multiplied by the thickness of each ply ($t_{ply} = 0.148\ mm$ – determined based on the complete laminate thickness after curing).

Table 2: Layup stacking sequence and equivalent longitudinal bending stiffness.

Stacking sequence	**Equivalent longitudinal bending stiffness, E_x^f (GPa)**
$[0]_8$	141
$[0/90_2/0]_S$	88.2
$[90/0_2/90]_S$	63.5
$[90/45/-45/0]_S$	22.2
$[90/60/90/-60/0]_S$	12.8

The prepregs were stacked by hand layup with intermediate debulking steps for 20 minutes in a sealed table under the pressure of around 100 mbar between added layers. The CFRP laminates were then cured in an autoclave on a flat aluminium plate covered with an A4000 high-performance fluoropolymer release film (Airtech International INC., USA) under 7 bars of pressure and 110°C for 60 minutes.

After curing, the cured CFRP plates were cut to the DCB substrates' dimensions. On the smooth side of the substrate (surface in contact with the aluminium plate during curing), the surface was then carefully manually sanded (400 grid sandpaper) in a criss-cross pattern and cleaned with a soaked acetone cloth. After that, the surface was exposed to artificial high-intensity U.V. lights in an in-house U.V./Ozone apparatus for 7 minutes, as described in [16], [30], to remove possible organic contaminants and modify the laminates' surface at a molecular level. It is worth mentioning that the total distance between the U.V. lamps and the laminates' surface was equal to 40 mm, and the adhesive's application was made immediately after the U.V./Ozone treatment.

Two adhesives with distinct fracture toughness were used to bond the composite substrates: the bi-component epoxy Araldite 2015/1 (G_{IC} = 640 J/m^2) [30], supplied by Huntsman International LLC, and the tougher epoxy film adhesive with a knit embedded carrier, AF 163 – 2K, supplied by 3M Scotch-Weld^{TM} (G_{IC} = 2416 J/m^2) [17]. The specific curing procedure of each adhesive is described in Table 3.

Table 3: Adhesive's curing description.

Adhesive	Time (minutes)	Temperature (°C)	Pressure (bar)	Method
AF 163- 2K	90	120	3	Autoclave
Araldite 2015/1	60	80	-	Oven

The DCB specimens' dimensions are detailed in Figure 1. A minimum thickness of 0.3 mm of the adhesive layer was ensured for the specimens bonded with the Araldite 2015/1 by metallic spacers positioned in both extremities of the DCBs bonded, and a minimum thickness of 0.25mm by the nominal thickness of the carrier embedded in the film adhesive AF 163-2k. Additionally, Teflon tape was used to produce an initial crack length of 35 mm.

Finally, loading blocks were bonded at the specimens' up and bottom surfaces using a bi-component epoxy adhesive Araldite 2012.

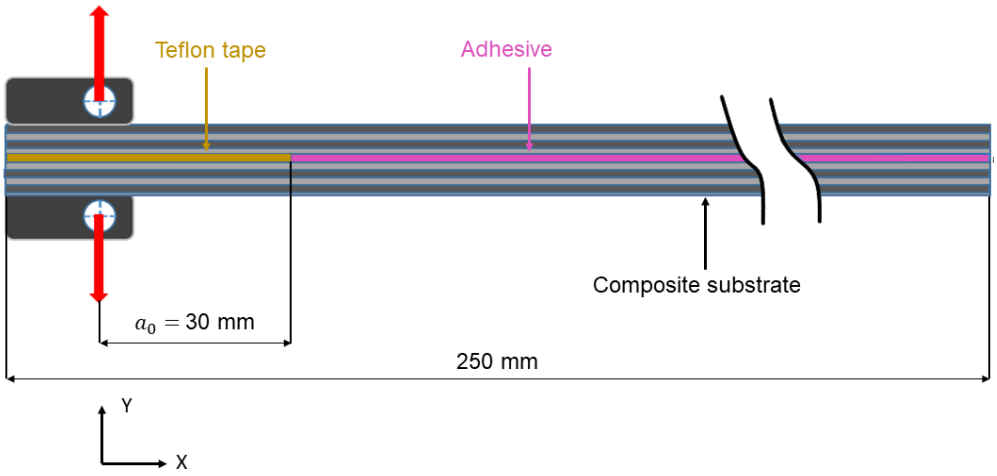

Figure 1: DCB specimen's dimensions, load conditions and initial crack length.

2.2 Experimental setup

A Zwick electro-mechanical testing machine with a 1 kN load cell was used to perform the DCB quasi-static tests under mode I loading. A testing speed of 4 mm/min was applied in all tests, as recommended by the standard ASTM D5528-13 [35]. The crack position was tracked during the tests by visual inspection of the specimen's lateral surface using a regular camera.

The analysed surface was white painted to improve the picture's contrast and crack-tip visualisation. At least four specimens of each test series were performed.

To better track the crack propagation paths, a travelling microscope was used to take photos of the free lateral surface of the specimen. Both regular and microscope cameras had the photos synchronised with load and displacement information from the testing machine and an acquisition frequency of 4 photos each second. The detailed experimental setup is shown in Figure 2.

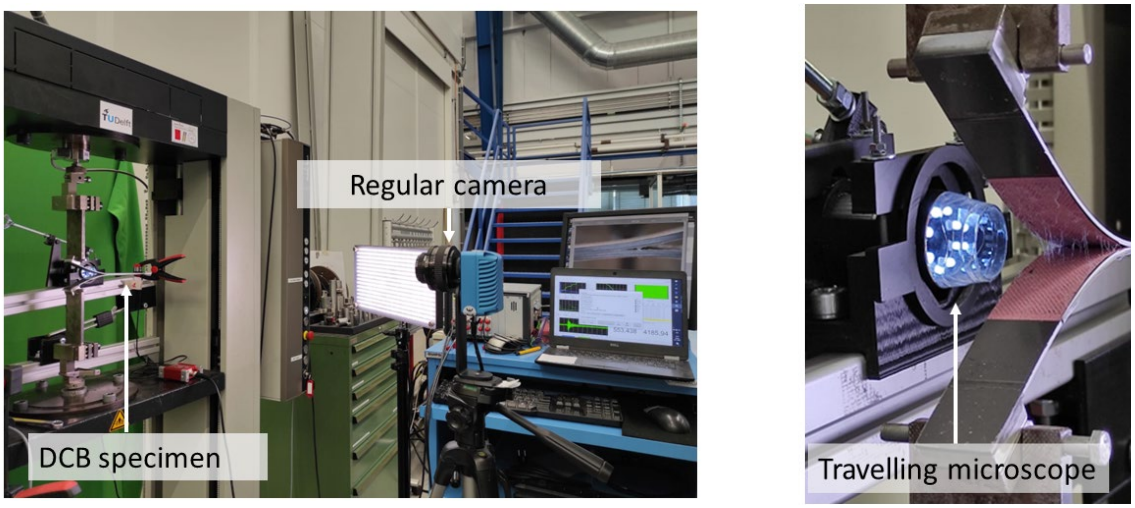

(a) (b)

Figure 2: (a) Experimental setup DCB tests and (b) detail showing the travelling microscope and a specimen $[0]_8$ bonded with adhesive AF 163-2k.

2.3 DCB test – calculation method

The fracture toughness of each specimen was calculated based on the Modified Beam Theory (MBT) data reduction method as recommended by the standard ASTM D5528-13 [35].

The following equation was used for this calculation:

$$G_I = \frac{3P\delta}{2b(a + |\Delta|)} \qquad \text{Eq. 02}$$

In which P is the load [N], δ is the displacement [mm] recorded by the testing machine during the tests, b and a correspond to the specimen's width and crack length visually measured,

respectively. The variable Δ represents a calibration parameter experimentally determined by the intercept of a least squares plot of the cube root of the specimen's compliance ($C^{1/3}$) as a function of the measured crack length, taking the compliance as the ratio between the load-point displacement to the applied load (δ/P).

2.4 X-ray micro CT

Selected DCB samples were observed through an X-ray micro CT scanner (Phoenix Nanotom, Waygate Technologies, Germany). Before scanning, the selected DCB samples were loaded, and the opening arms were fixed using a metallic insert to keep them opened for ex-situ observations. The reconstructed 3D model had a voxel size of 12.5 μm.

2.5 Finite element model

A 3D finite element model based on continuum Cohesive Zone Elements (CZE) was created to predict the crack onset and aid in the understanding of the damage mechanisms of the DCB joints under quasi-static pure mode I loading using the commercial ABAQUS software version 2020.

The eight-node brick elements (C3D8) were used to model the CFRP substrate and adhesive materials. The cohesive failure within the adhesive layer, the composite delamination between the composite plies and the matrix cracking within each composite ply were simulated using the eight-node three-dimensional cohesive elements (COH3D8). It is worth mentioning that no distinction is made between the adhesive and the cohesive failure in the adhesive joint. A bi-linear traction separation law was implemented into the model to predict crack growth and degradation based on the maximum nominal stress criteria.

The properties of the materials used in the finite element analysis are described in Tables 4 and 5. The proposed values are based on the materials' data sheet at room temperature (25°C). It is worth mentioning that a stiffness value of 10^6 was applied for the cohesive elements to avoid elements degradation in undesired regions, as recommended in [36], [37].

Table 4: Material properties used solid elements in the finite element analysis.

Material	**E_{11} (MPa)**	**E_{22} - E_{33} (MPa)**	**V_{12} - V_{13}**	**V_{23}**	**G_{11}- G_{22} (MPa)**	**G_{33} (MPa)**
Hexply 8552 – AS4[a]	141000	9750	0.267	0.5	5200	3190
Adhesive layer	15000	-	0.45	-	-	-

Table 5: Properties used in the cohesive zone elements at the interfaces applied in the finite element analysis.

Material	**E (MPa)**	**G_{Ic} (J.m^{-2})**	**σ (MPa)**
Hexply 8552 – AS4	1.0E6	500[a]	64[a]
Araldite 2015/1	1.0E6	500[b]	22[c]
AF 163- 2K	1.0E6	2416[d]	46[e]

[a] Technical data sheet Hexply 8552 – AS4 [34].

[b] Technical data sheet Araldite 2015/1 [38].

[c] N. P. Lavalette et al. [39].

[d] S. T. de Freitas et al. [16].

[e] J. Kupski et al. [11].

Figure 3 shows an example of the cohesive element layers distribution in the $[90/0_2/90]_s$ specimen. As can be seen, three different cohesive layers with a very thin thickness (5 microns) were created: The first one (pink colour) is located in the middle of the bondline representing a purely cohesive failure (1); the blue lines represent the delamination between the composite plies being located at the interface of each composite ply in the longitudinal direction (2); the green lines are located in the transversal direction of the 90° degree plies, next to the crack tip region to simulate transversal matrix cracking (3). It is important to note that, for the sake of simplicity, the cohesive element has only been introduced in the first 90° ply. In fact, the objective here is to study the competition between the propagation of the crack in the adhesive and the creation of a new crack in the composite.

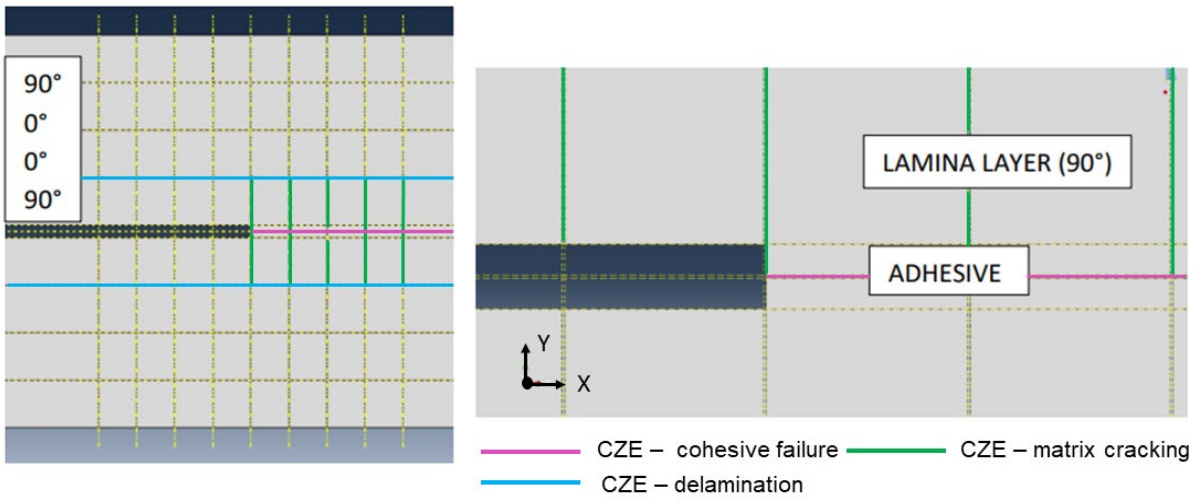

Figure 3: Example of the cohesive zone elements (CZE) distribution in $[90/0_2/90]_s$ finite element analysis: (1) pink lines CZE representing cohesive; (2) blue lines CZE representing delamination and (3) green lines CZE representing the transverse matrix cracking.

A mesh convergence study was performed to identify an ideal mesh size that guaranteed mesh-independent results with minimum computational efforts. A mesh size of 0.5 mm near the crack tip and 1 mm near the loading point was implemented. Figure 4 shows the boundary and loading conditions of the model, which consisted of: on the specimen's right-hand side (Reference Point – RP1), the 3 degrees of freedom were set to zero (encastre) and on the specimen's left-hand side (Reference Point – RP2 and RP3) a constant vertical displacement in its free end (the other degrees of freedom were kept equal to zero).

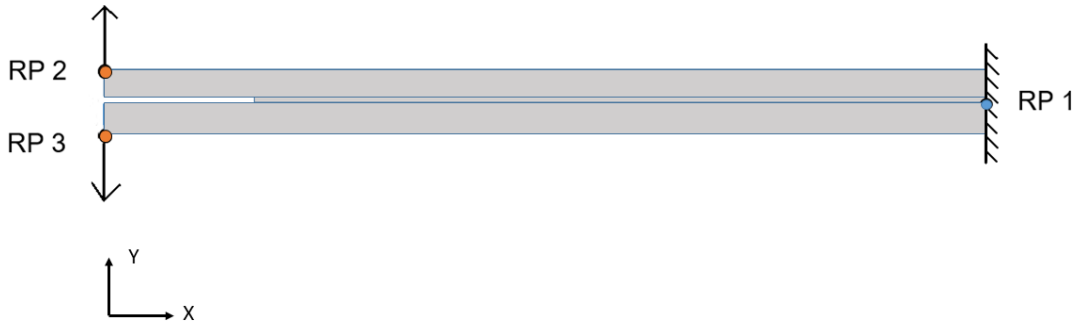

Figure 4: Scheme boundary conditions numerical model.

3 Experimental results

Figure 5 shows representative load versus displacement curves of the DCB specimens bonded with the AF 163-2k -Figure 5(a) and Araldite 2015/1 - Figure 5(b) for the five different CFRP layups. The maximum load value before crack propagation was observed in the 0-degree unidirectional specimens (black line) for both adhesive types, approximately 140 N and 50 N for the AF 163-2k and Araldite 2015/1, respectively.

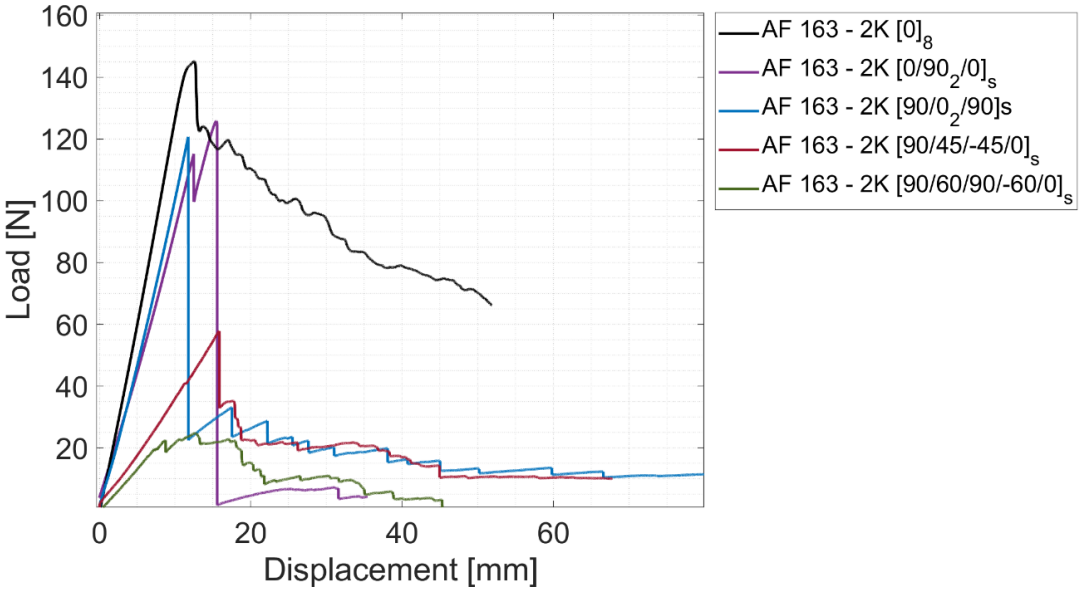

(a)

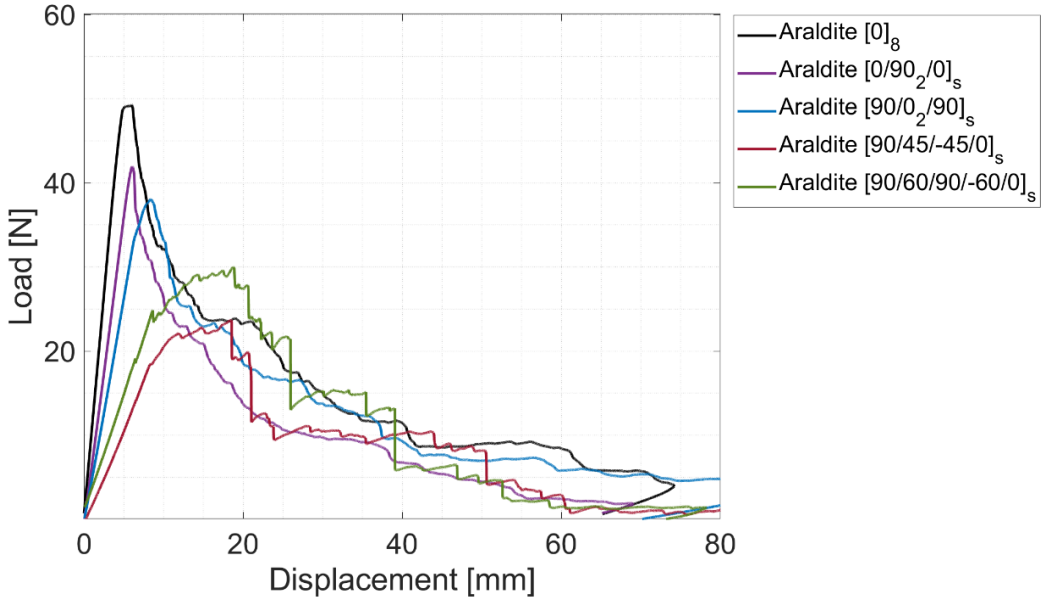

(b)

Figure 5: Load versus displacement curves (a) AF163-2k and (b) Araldite 2015/1 adhesive.

Observing the load versus displacement curves, it is also worth mentioning that the initial stiffness of the curves is different for all specimens due to the different bending stiffness of the layups (see Table 2). As expected, the steepest slope in the linear response region corresponds to the layup with the highest longitudinal bending stiffness $[0]_8$, followed by the $[0/90_2/0]_S$ and $[90/0_2/90]_s$ with lower slopes. The joints with the $[90/45/-45/0]_S$ and $[90/60/90/-60/0]_S$ layups present the lowest stiffness and a considerable reduction in the maximum load values.

The specimens bonded with the tougher adhesive, AF 163-2k, showed significant differences in the post-peak responses for each type of substrate's CFRP layup, indicating different fracture mechanisms. Figure 6 shows the representative fracture surfaces for each layup. All specimens AF163-2K_$[0]_8$ presented a cohesive crack propagation within the bondline that resulted in the gradual decrease in the load versus displacement curve after the maximum load – see Fig. 5a. All the remaining layups presented a fracture surface within the composite substrate, mostly delamination. This led to a sudden drop in the load values in most cases, with the exception of [90/60/90/-60/0]s layup.

Overall in this particular adhesive, when the interface ply angle was larger than 0-degrees, the crack path deflected (by crack kinking or initiation of a new crack in the adjacent ply) from the bondline into the composite until encountering the first 0-degree ply, where the crack propagated further by delamination. This was also observed by Kupski *et al*. [37] in single lap bonded joints and by Khan *et al*. [30] in double lap and flat-wise tensile joints.

As shown in Figure 6, , the crack deflection through the composite for the specimens with $[90/45/-45/0]_s$ and $[90/60/90/-60/0]_s$ layups is even more evident as the crack migrates until the midplane of the composite substrate(crack depth from 1st to 4th and 5th layers, respectively). Due to the crack path deflection into the laminate, the opening of DCB specimens was no longer symmetric, leading to a twisting curvature of bonded CFRP parts.

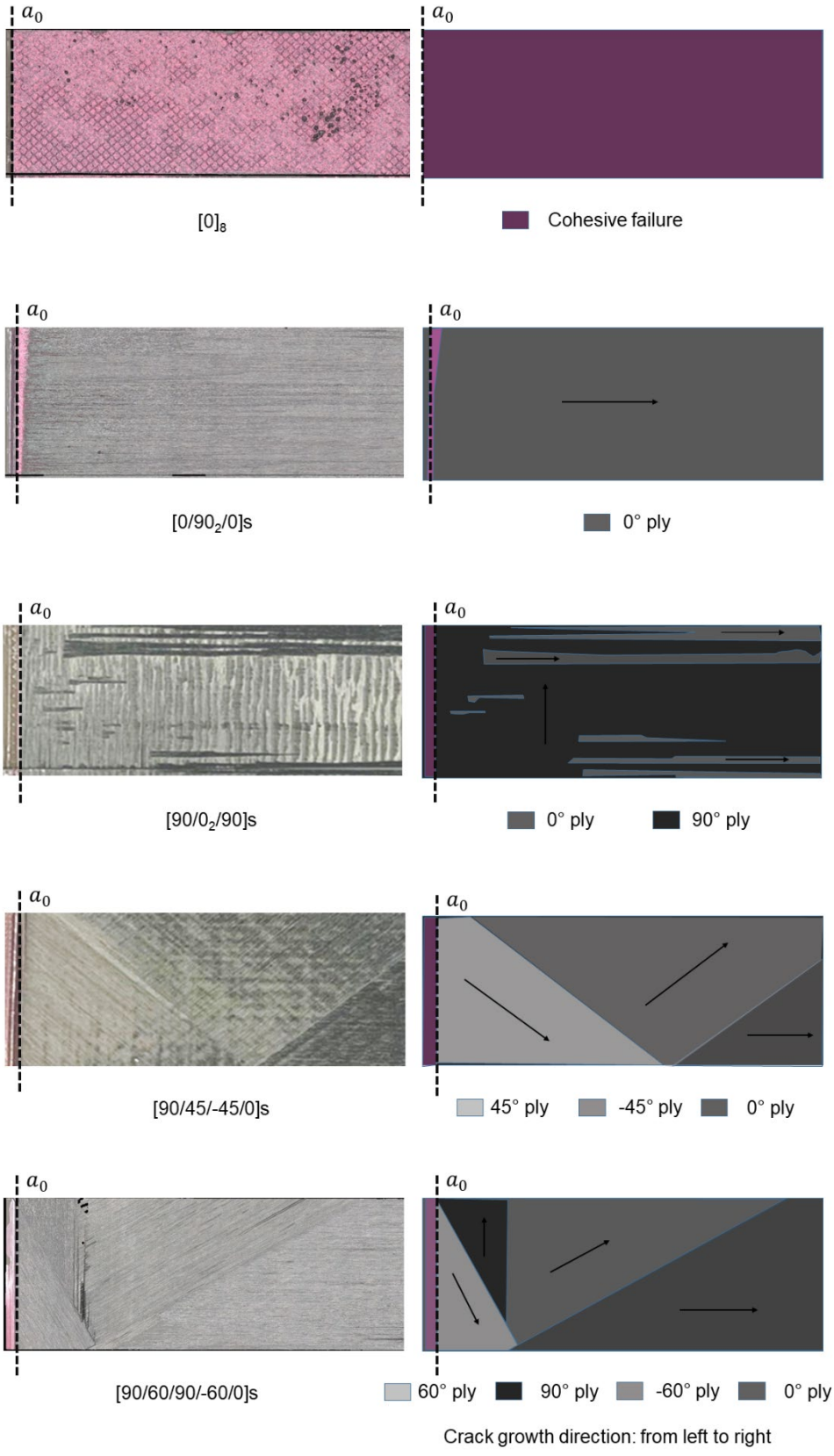

Figure 6: Representative fracture surface of the AF163-2K DCB specimens (photos on the left-hand side and schematics of the fracture and ply angles on the right-hand side)

Figure 7 shows the representative fracture surfaces of the specimens bonded with Araldite 2015/1. The layups $[0]_8$, $[0/90_2/0]_S$, and $[90/0_2/90]_S$ showed cohesive failure and similar trends of the load versus displacement curves with a gradual decrease of the load after the maximum value.

For the specimens with $[90/45/-45/0]_S$ and $[90/60/90/-60/0]_S$ layups, the crack deflected into the composite substrate until reaching the 0-degree ply delamination - identically to what was observed with the adhesive AF 163-2K. It is worth mentioning that for the specimens bonded with the Araldite, the specimen $[90/45/-45/0]_S$ actually presented lower stiffness when compared with the [90/60/90/-60/0]s specimen, conversely from what was calculated and present in table 2. A possible reason for this behaviour is the crack onset of the Araldite_$[90/45/-45/0]_S$ within the bondline (see Figure 7), followed by crack deflection into the composite substrate, that was not present in the AF163-2K_$[90/45/-45/0]_S$.

Figure 8 shows the R-curves for each corresponding load versus displacement curve presented in Figure 5. The fracture toughness of the DCB joint was determined by Equation 02 as recommended by the standard ASTM D5528-13.

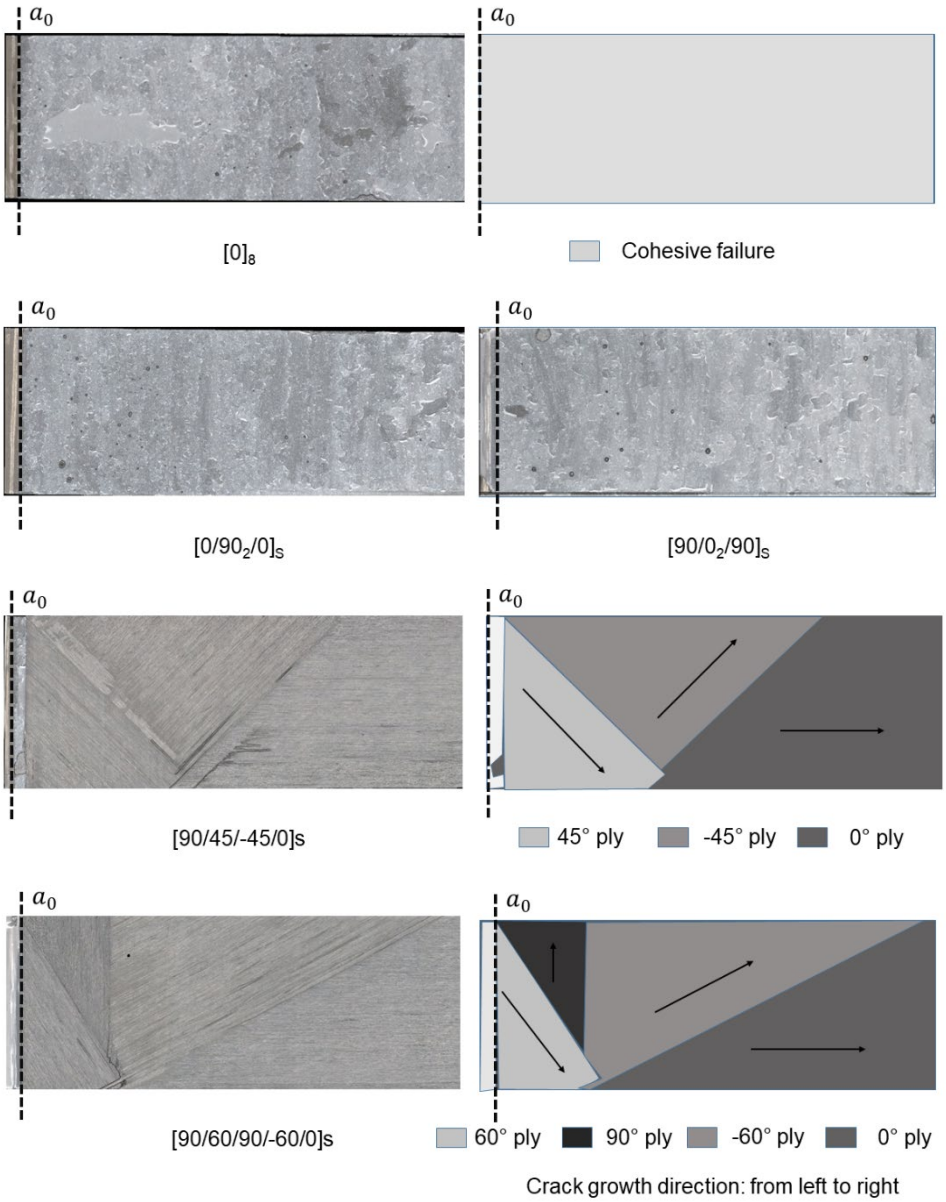

Figure 7: Representative fracture surface of the Araldite 2015/1 DCB specimens (photos on the left-hand side and schematics of the fracture and ply angles on the right-hand side). In the second row only photos are shown since both specimens presented a cohesive failure.

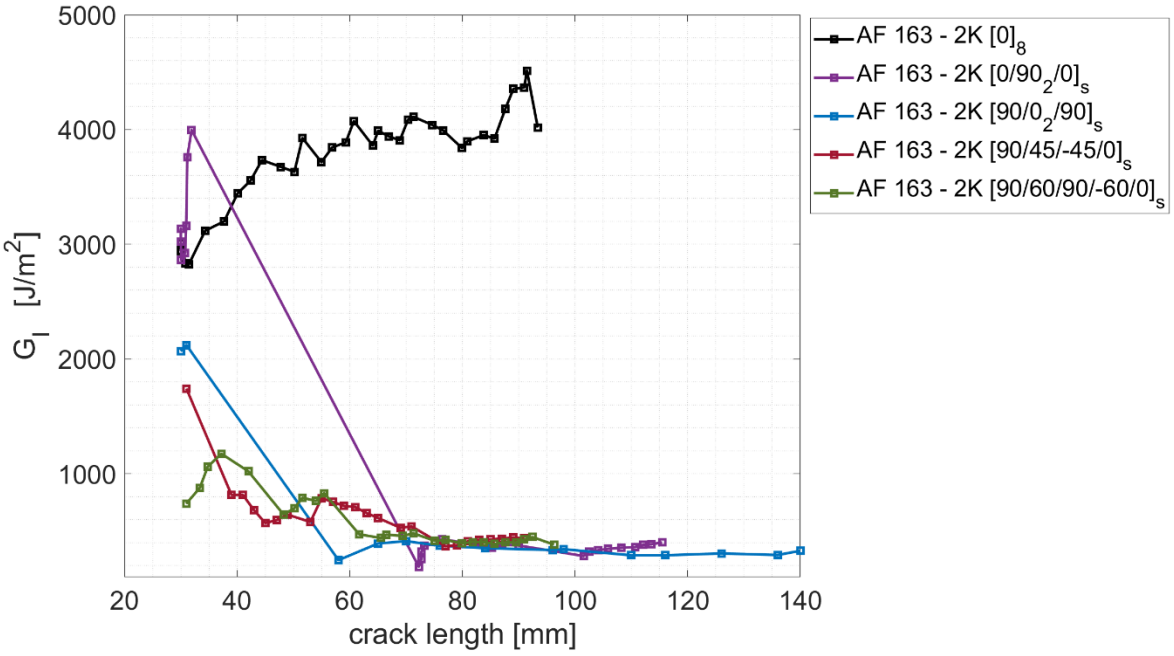

(a)

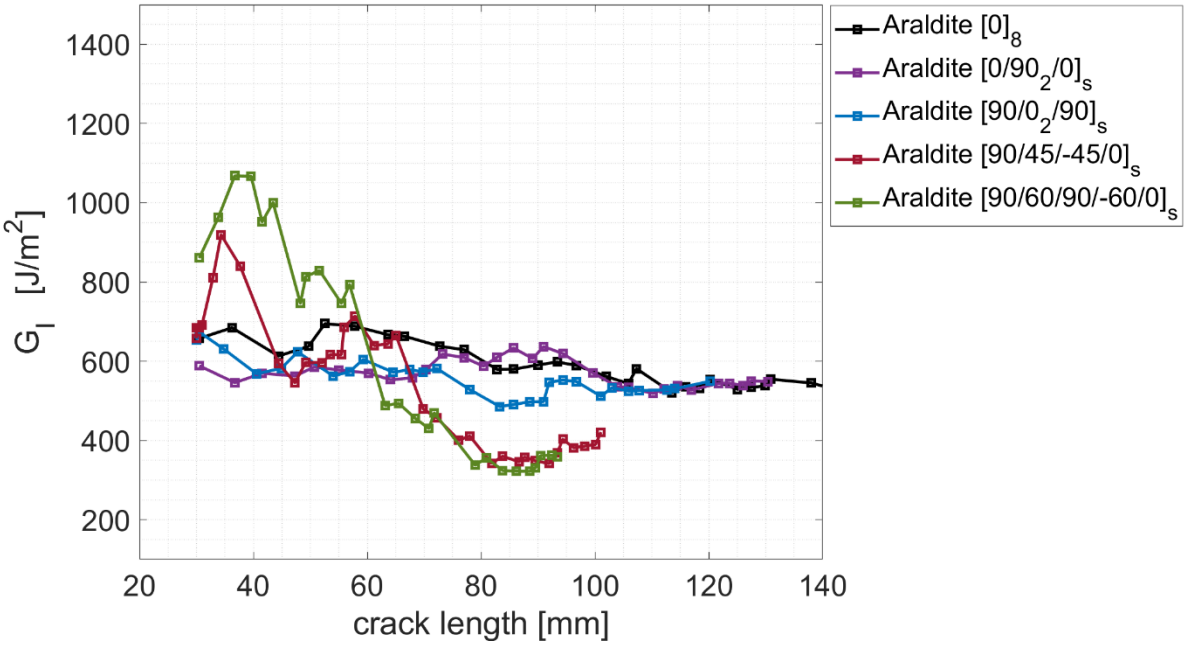

(b)

Figure 8: R-curve of DCB specimens bonded with (a) AF 163-2k and (b) Araldite 2015/1 adhesive.

As seen in Figure 8 (a), the energy release rate of the AF 163-2k_$[0]_8$ unidirectional joint (black line) is stable but increases during crack propagation as a function of the crack length. The fracture toughness at onset value is approximately 2800 J/m^2. This is approximately 15% higher than the fracture toughness at onset reported by [16] for the same adhesive and 45% higher than for the same adhesive without a carrier (AF163-2U – unsupported), reported in [40]. For the AF163-2k_$[0/90_2/0]_S$ and AF163-2k_$[90/0_2/90]_S$ specimens, a high peak characterises the R-curve at the damage onset region (GI equals to 3568 and 2147 J/m^2, respectively) followed by a sudden drop in the G_I value to a plateau around 300 J/m^2 as the crack propagates. Of particular interest is the AF163-2k_$[0/90_2/0]_S$ joint's onset fracture toughness which is 25% higher than the one shown in the unidirectional specimen AF163-2k_$[0]_8$.

Figure 8 (b) shows the R-curve using Araldite 2015/1 – a low-toughness adhesive. A stable crack propagation is observed in the specimens with cohesive failure within the bondline, i.e., Araldite_$[0]_8$, Araldite_$[0/90_2/0]_S$ and Araldite_$[90/0_2/90]_S$. The average value fracture toughness measured in these specimens is 600 J/m^2, which is in accordance with Araldite 2015/1 nominal fracture toughness specified by the supplier (between 400-600 J/m^2) [39].

For both adhesives, the R-curves of the $[90/45/-45/0]_S$ and $[90/60/90/-60/0]_S$ specimens have a wavy shape (peaks and valleys before the plateau) which will be discussed in more detail in section 5. It is out for notice that the $[90/60/90/-60/0]_S$ specimens bonded with the adhesive Araldite 2015/1 present a 97% increase of the fracture toughness onset (G_I = 1183.3 J/m^2) when compared with the $[0]_8$ specimens.

4 Numerical results

Another relevant tool to better understand the damage mechanisms within the proposed joints and the different paths undertaken by the crack is the Finite Element Analysis (FEA). A failure criterion based on the linear-elastic fracture mechanics was used to predict the crack onset for each studied composite layup. Following this criterion, once initiated, the crack can propagate if the energy release rate is greater than the toughness. Table 6 compares the crack onset behaviours observed experimentally and using the finite element analysis. In addition, the joint's onset energy released rate is summarised.

Table 6: Specimens' mode I fracture toughness and the crack onset location obtained experimentally and by finite element analysis.

Adhesive type	**CFRP stacking sequence**	**G.I. (J/m2) at the crack onset (average ± standard deviation)**		**Crack onset location** (Experimental)	**Crack onset location** (FEA)
AF 163 – 2K	$[0]_8$	2868	± 195.4	adhesive	adhesive
	$[0/90_2/0]s$	3568	± 322.2	adhesive followed by matrix cracking	adhesive and composite layup
	$[90/0_2/90]s$	2147	± 306.1	composite layup	adhesive and composite layup
	$[90/45/-45/0]_S$	1400	± 435.4	composite layup	composite layup
	$[90/60/90/-60/0]_S$	1033.3	± 28.9	composite layup	-
Araldite 2015/1	$[0]_8$	619.7	± 44.76	adhesive	adhesive
	$[0/90_2/0]s$	563.9	± 79.6	adhesive	adhesive
	$[90/0_2/90]s$	600.1	± 58.8	adhesive	adhesive
	$[90/45/-45/0]_S$	780	± 71.2	adhesive and composite layup	adhesive and composite layup
	$[90/60/90/-60/0]_S$	1183.3	± 155.5	composite layup	-

For the tougher adhesive AF 163-2K , the adherend layup strongly influenced the joint's G_I onset values since its transversal strength seems to be competitive compared with the composites. It is worth to notice that the highest fracture toughness at crack onset was achieved when using the layup _$[0/90_2/0]_S$. This layup outperformed the cohesive failure crack onset by 25% (AF 163-2k_$[0/90_2/0]_S$ 3568 J/m^2) when compared with the AF 163-2k_$[0]_8$ 2868 J/m^2). Further analysis on the reason behind this improvement are described in the discussion section.

The Araldite 2015/1 adhesive with lower fracture toughness presents a cohesive failure in most studied cases, showing that the preferential path for crack propagation was the bondline. The Araldite_$[0]_8$, Araldite_$[90/0_2/90]_S$, and Araldite_$[0/90_2/0]_S$ specimens that presented a cohesive failure present a G_I value of around 600 J/m^2. For the layups with 45 and 60-degree plies orientation where the fracture occurred within the composite substrate, the fracture toughness of these joints was higher than the fracture toughness of the intralaminar CFRP (300 J/m^2) and the cohesive failure of the adhesive Araldite (600 J/m^2).

5 **Discussion**

To better understand the influence of the composite's layups on the fracture behaviour of composite bonded joints under mode I loading, the crack propagation paths were closely looked for each crack increment. The Load and displacement (L-d) curves and R-curves of each test series were then correlated with the crack propagation paths. This discussion section is divided into three main subgroups of laminate: unidirectional laminate, cross plies and multidirectional layups.

5.1 Unidirectional laminate $[0]_8$

As previously observed, all specimens with $[0]_8$ as substrates, AF 163-2k_$[0]_8$ and Araldite_$[0]_8$ presented cohesive failure. The specimens bonded with the Araldite presented a stable and almost constant R-curve with a G_I value of around 600 J/m^2, see Figure 8(b). However, AF 163-2k_$[0]_8$ presented a linear increase of the R-curve during the mode I crack propagation, as detailed in Figure 9 (a). Figure 9 (b) shows the images taken from the travelling digital microscope of the two highlighted points in the R-curve.

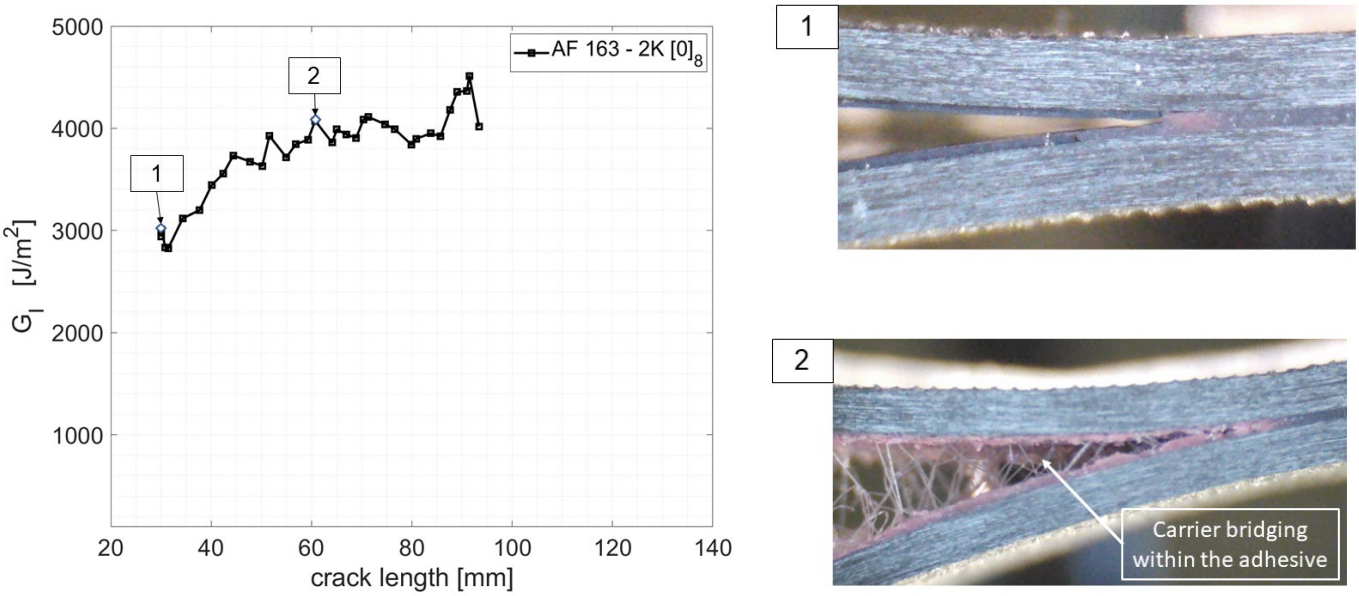

(a) (b)

Figure 9: (a) Detailed R-curve of AF 163-2k_$[0]_8$ specimen and (b) lateral images taken from the travelling microscope in points 1 and 2.

As seen in Figure 9 (b), the cohesive failure of the AF163-2k adhesive and a carrier pull-out was observed throughout the complete crack length. This carrier pull-out resulted in crack bridging and increased the energy needed to open an increment of the crack as the crack progressed. As a result, the G_I value increased in every crack increment: increasing the joint's fracture toughness from about 3000 J/m^2 in point 1 to 4000 J/m^2 in point 2 (an increase of 33%).

Figure 10 shows Micro CT images of one of the DCB coupons. As it can be observed, the carrier bridging occurred throughout the entire specimen width, in which the carrier wires were pullout from the adhesive layer while the crack propagated. This toughening mechanism occurs behind the crack tip, i.e., it is only triggered after the crack has propagated. The carrier bridging worked as an extrinsic toughening mechanism of the adhesive joint with an increase of toughness in an average of 24 J/m^2 at each 1 mm crack length increment. A similar extrinsic toughening mechanism was also observed in [30] with the same type of adhesive.

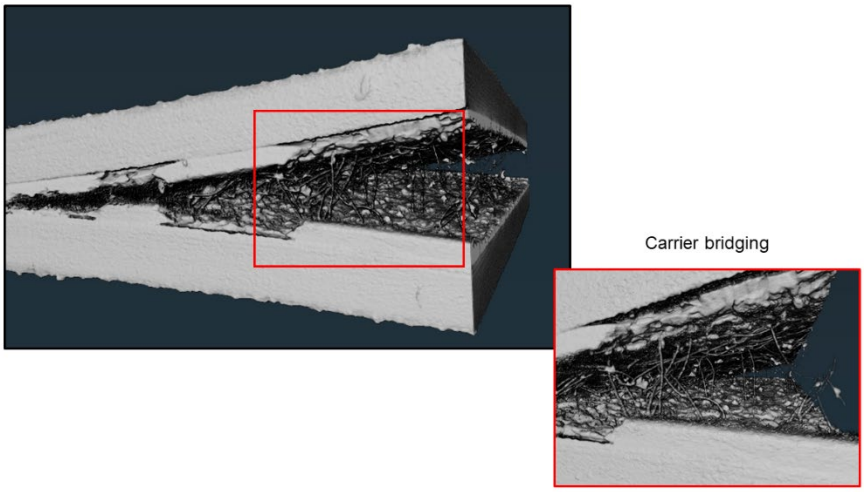

Figure 10: Micro CT images of specimen AF 163-2k_$[0]_8$.

5.2 Cross-ply laminates $[0/90_2/0]_S$ and $[90/0_2/90]_S$

For the cross-ply laminates, each adhesive presented utterly different results. The specimens bonded with Araldite 2015/1 adhesive presented cohesive failure, as previously observed in Figure 7, while AF163-2k_$[0/90_2/0]_S$ and AF163-2k_$[90/0_2/90]_S$ specimens presented damage mechanisms mainly characterised by matrix cracking and delamination.

To better understand these differences and the influence of the adhesive's type in the crack propagation paths within the joints, the stiffness degradation of the different CZE (see Figure 3) is shown in Figure 11. It is worth mentioning that the arrows in Figure 11 represent:

- Green – represents the crack propagation within the adhesive layer;
- Red – represents crack deflection through the composite layups;
- Blue – paths with an increase in the cohesive elements' stiffness degradation – regions of stress concentration;

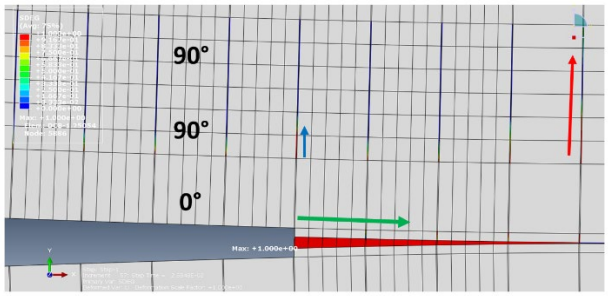

(a) AF 163-2k_$[0/90_2/0]$s

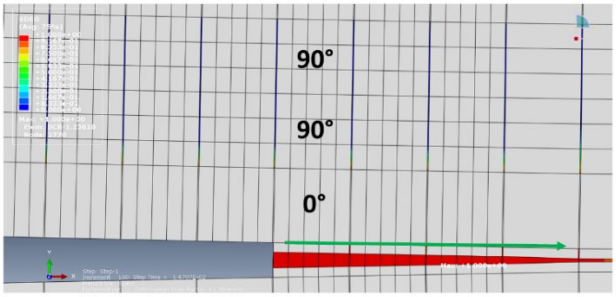

(b) Araldite_$[0/90_2/0]$s

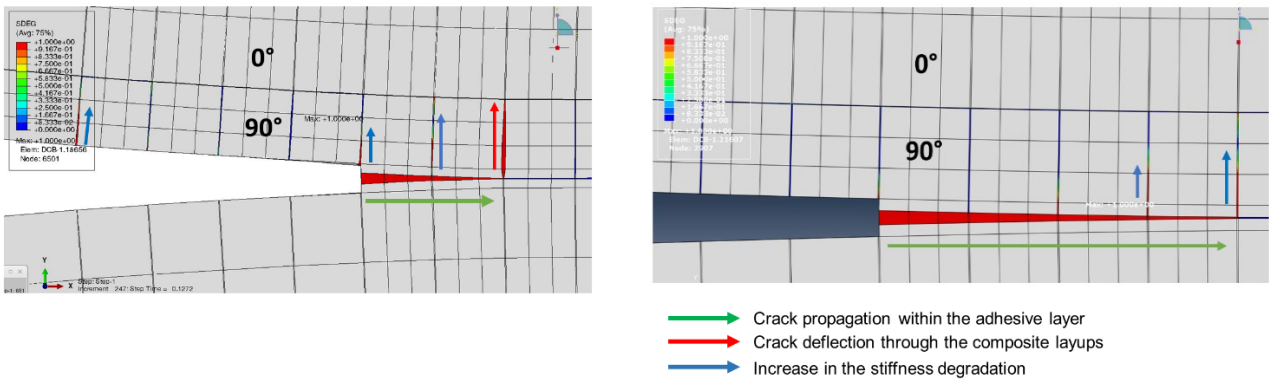

(c) AF 163-2k_[90/0_2/90]s (d) Araldite_[90/0_2/90]s

Figure 11: CZE stiffness degradation predicted by FEA of specimens [0/90_2/0]s bonded with adhesives (a) AF 163-2K and (b) Araldite 2015/1; [90/0_2/90]s bonded with adhesives (c) AF 163-2K and (d) Araldite 2015/1. (colours transition from blue to red, that is, from undamaged to completely damaged).

In the case of the AF163-2K_[0/90_2/0]$_S$ and AF163-2K_[90/0_2/90]$_S$ specimens in Figures 11 (a) and (c), the mechanism of crack competition is more evident since local stress singularities can be seen in different regions of the laminates' layup (represented by regions with higher stiffness degradation – blue arrows). The crack propagates until the local stresses finally overcome the adhesive's (green arrows) or the laminate's transversal strength (red arrows). So, for these specimens, a co-occurrence of multiple damage mechanisms (i.e., cohesive failure, matrix cracking and delamination) was triggered by the 90/0-degree layup combined with a tough adhesive.

For the [0/90_2/0]$_S$ and [90/0_2/90]$_S$ specimens bonded with the adhesive Araldite 2015/1 (Figures 11 (b) and (d) respectively), the stresses singularity at the crack-tip of the adhesive is predominant, leading to a cohesive failure onset.

Hereby we would like to pay particular attention to the specimens AF163-2K_[0/90_2/0]$_S$ fracture phenomena. This layup resulted in the highest toughness at crack onset, overcoming the crack onset of cohesive failure with [0]$_8$ layup. Figure 12 highlights four points in the L-d curve and corresponding R-curve to explain the increase in the joint's fracture toughness, see Figure 12 (a) and (b). Figure 12 (c) shows the corresponding microscopic images of the region close to the crack tip at those four points.

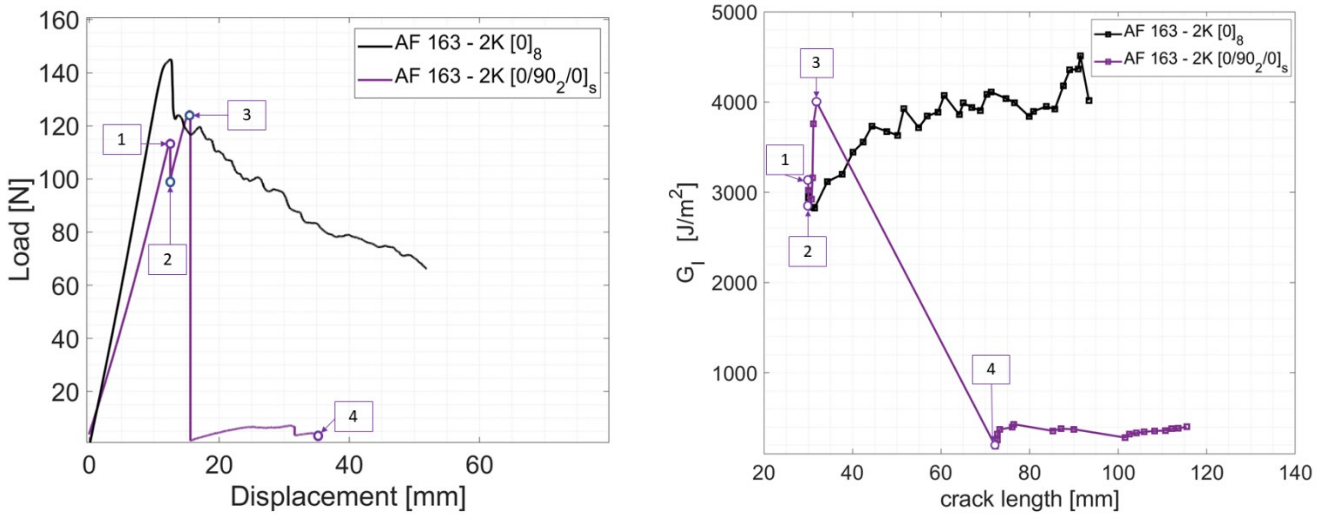

(a) (b)

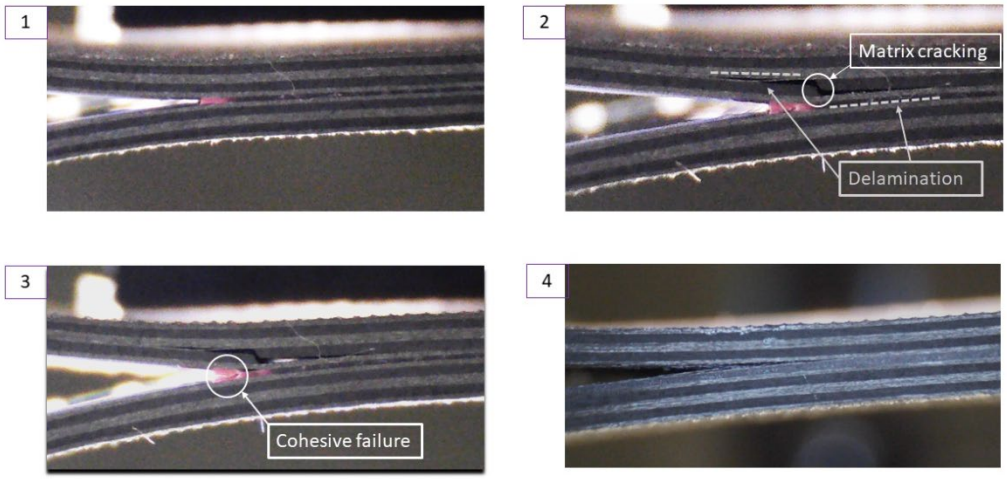

(c)

Figure 12: Detailed crack propagation paths of specimen AF 163-2k $[0/90_2/0]_S$ and $[0]_8$ and corresponding points at the load-displacement and R-curve.

From the images and correspondent L-d test output of Figure 12, we can observe that:

1. First peak in the load: No visible damage is yet identified;
2. First sudden decrease in the load: matrix cracking at the 90 degrees plies (the 2nd and 3rd from the bondline) is observed, followed by cracking propagation to the interface between the 0 degrees interface layer (1st ply from the bondline) and the 0 degrees at

the symmetry plane (4th ply from the bondline), leading to a z shape crack depicted in Figure 8 (d) – detail 2;

3. Increasing the load from point 2 to 3: represents the crack competition between the delamination between the 0-90 plies triggered by the matrix cracking and crack propagation inside the adhesive layer, i.e., cohesive failure;
4. A second sudden decrease in the load: delamination within the 0-degree interface ply (next to the bondline).

The fracture phenomena described above lead to an enhancement of approximately 25% at the fracture onset of AF163-2k_[0/90_2/0]s compared with the cohesive failure in AF163-2k_$[0]_8$. The composite layup properties, combined with the stress singularities of the pre-existing crack tip, lead to a crack competition phenomenon at the fracture onset in which multi-damage mechanisms co-occur, from matrix cracking to cohesive failure and crack deflection to the 0-90 degrees interface ply.

Higher energy is therefore required to overcome this competition until a more energetically favourable crack path is pursued. In this specific case, the delamination at the 0-degree ply and, consequently, the reduction in the G_I values.

Figure 13 shows the topography images of the final fracture surface of the AF163-2K_$[0]_8$ and AF163-2k_[0/90_2/0]$_S$ specimens with a colour scale from 0 to 1 mm, performed using the Keyence VR 5000 wide-area 3D profiling system. The lower limit (zero value) was defined based on the free surface of the specimen (without adhesive) and is defined as the baseline for all specimens. As can be observed in Figure 13 (a), the cohesive failure of specimen AF163-2k_$[0]_8$ is almost on the adhesive midplane, represented by the almost uniform dark blue colour. For AF163-2k_[0/90_2/0]$_S$ in Figure 13 (b), it is possible to see clearly a tiny region (violet colour) that represents a small propagation within the adhesive layer, followed by a delamination in the 0° ply, confirming the observations took during the analyses of the images of the travelling microscope.

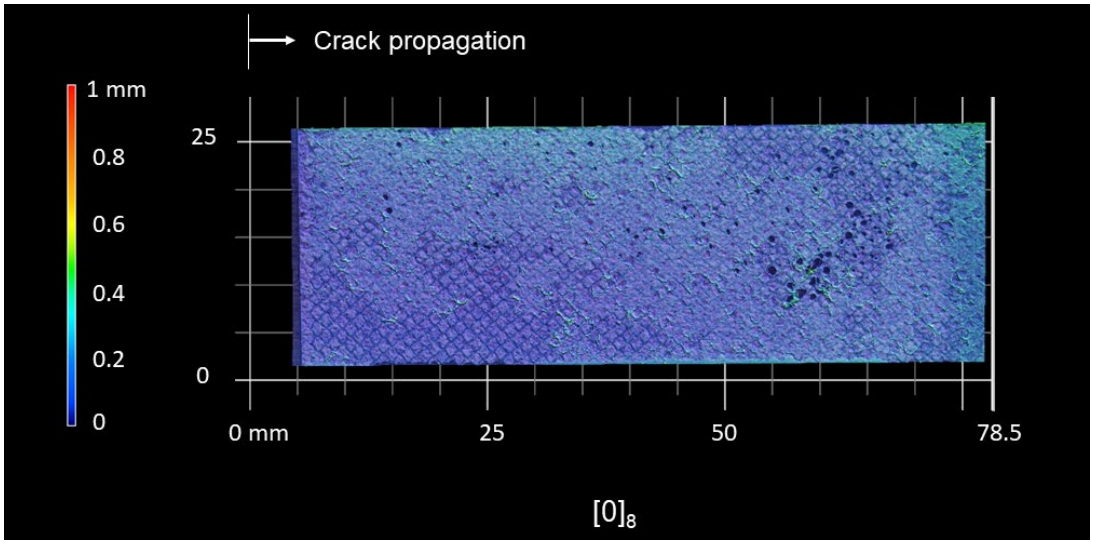

(a)

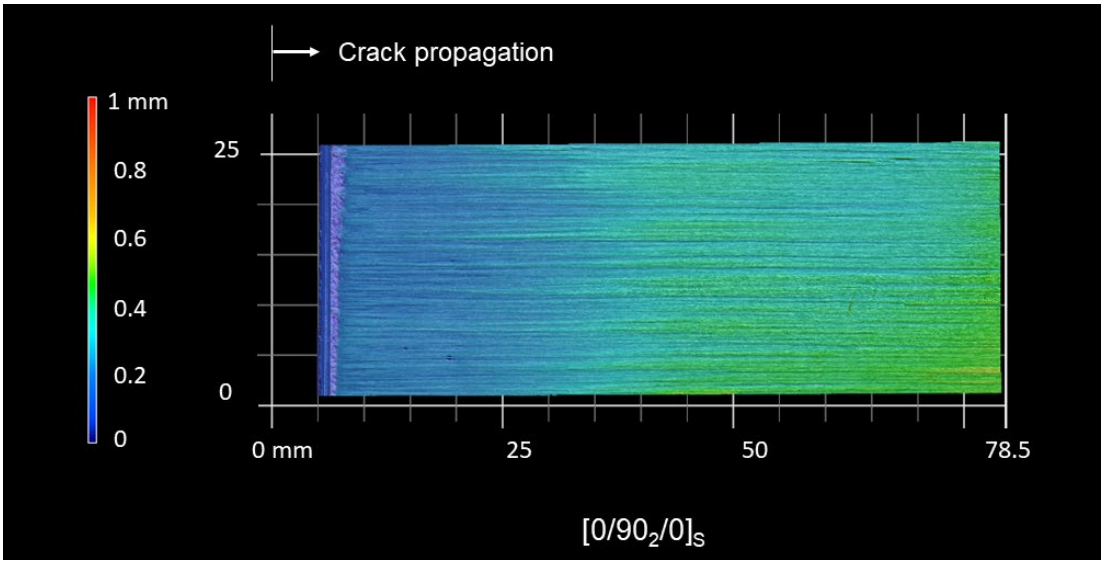

(b)

Figure 13: Topography of the fracture surface of specimens (a) AF163-2k_$[0]_8$ and (b) AF163-2k_$[0/90_2/0]_S$.

5.3 Multidirectional laminates $[90/45/-45/0]_S$ and $[90/60/90/-60/0]_S$

For the multidirectional laminates, two main observations will be hereby discussed. The first is the reasoning behind the wavy shape observed in the R-curve of both multidirectional laminates in both adhesives – see Figure 8. The second one is the influence of the adhesive type on the different crack onsets observed for the specimens with 45-degree ply – see Table 6.

Figures 14 and 15 show the R-curve, the images from the lateral of the specimens taken by the travelling digital microscope and the topography images of the fracture surfaces for the specimens Araldite_[90/45/-45/0]$_S$ and Araldite_[90/60/90/-60/0]$_S$, respectively.

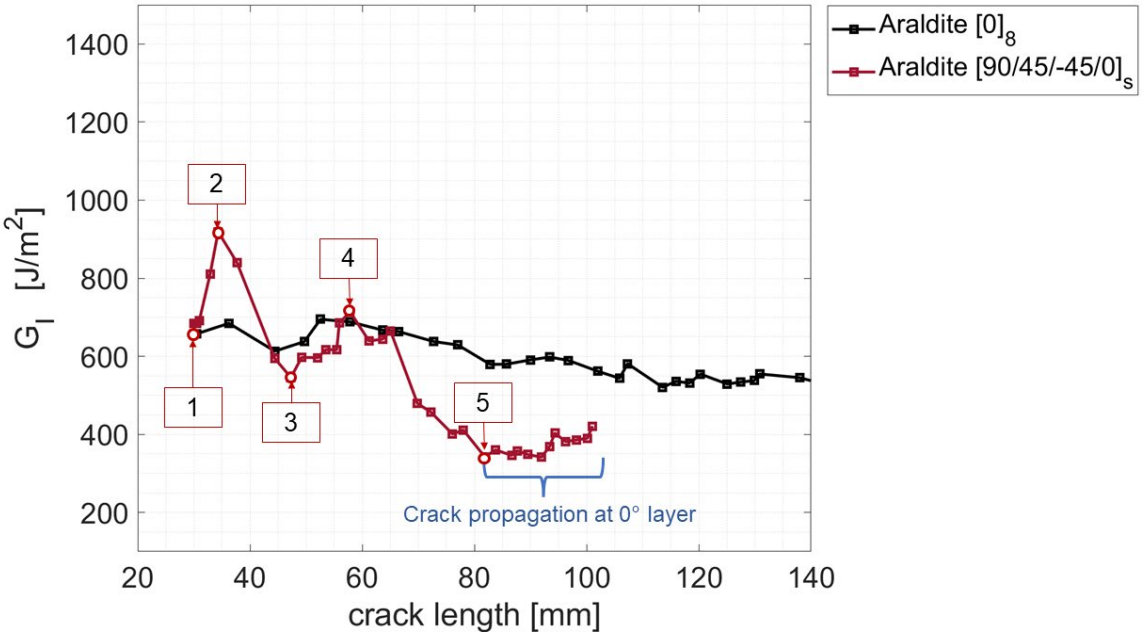

(a)

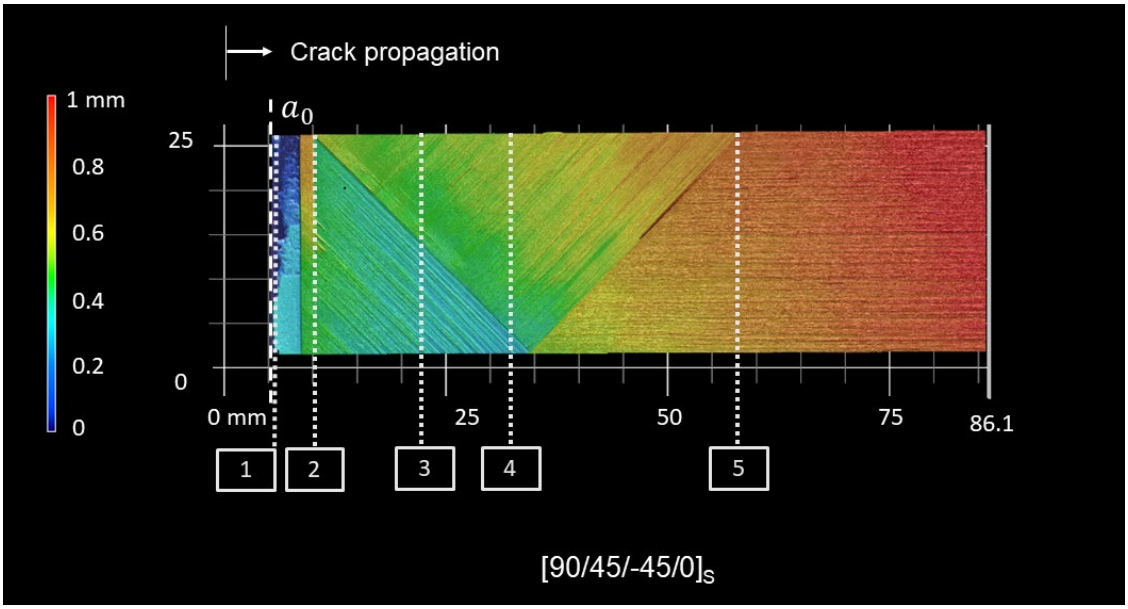

(b)

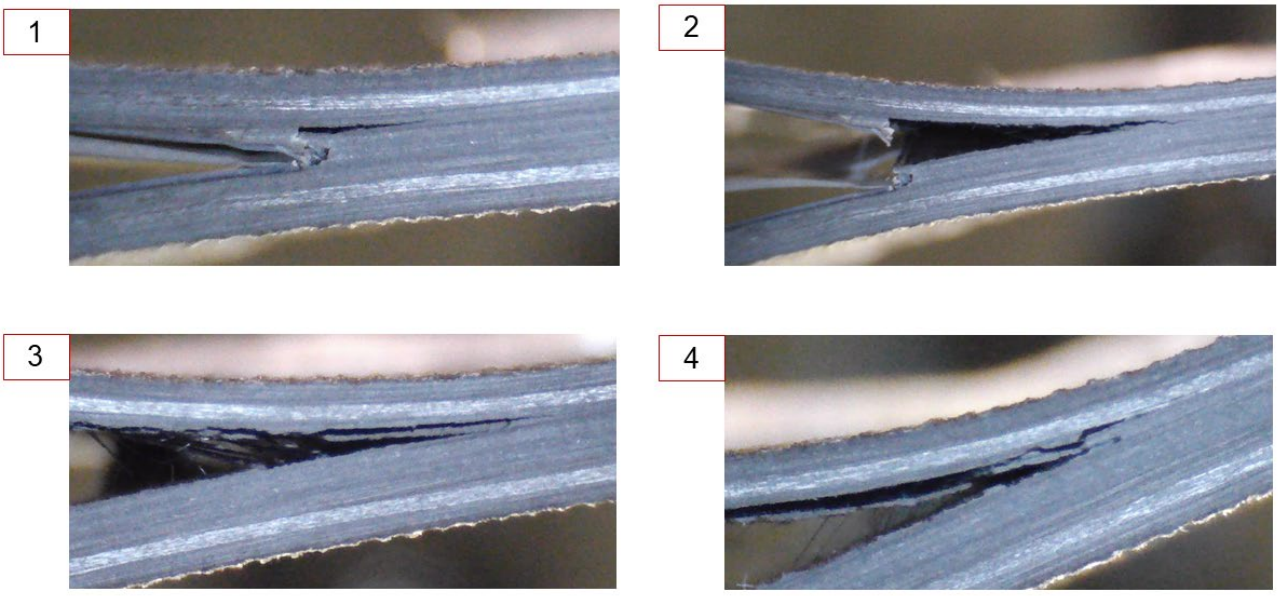

(c)

Figure 14: (a) R-curve, (b) topography and (c) images taken by the travelling microscope of the specimen Araldite_[90/45/-45/0]s.

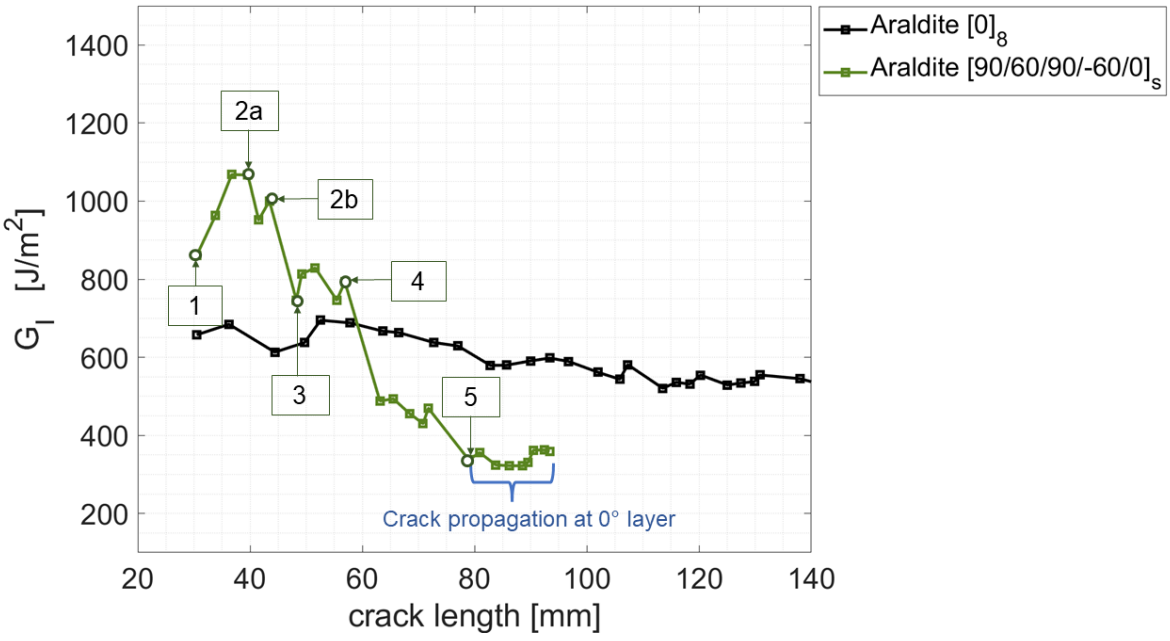

(a)

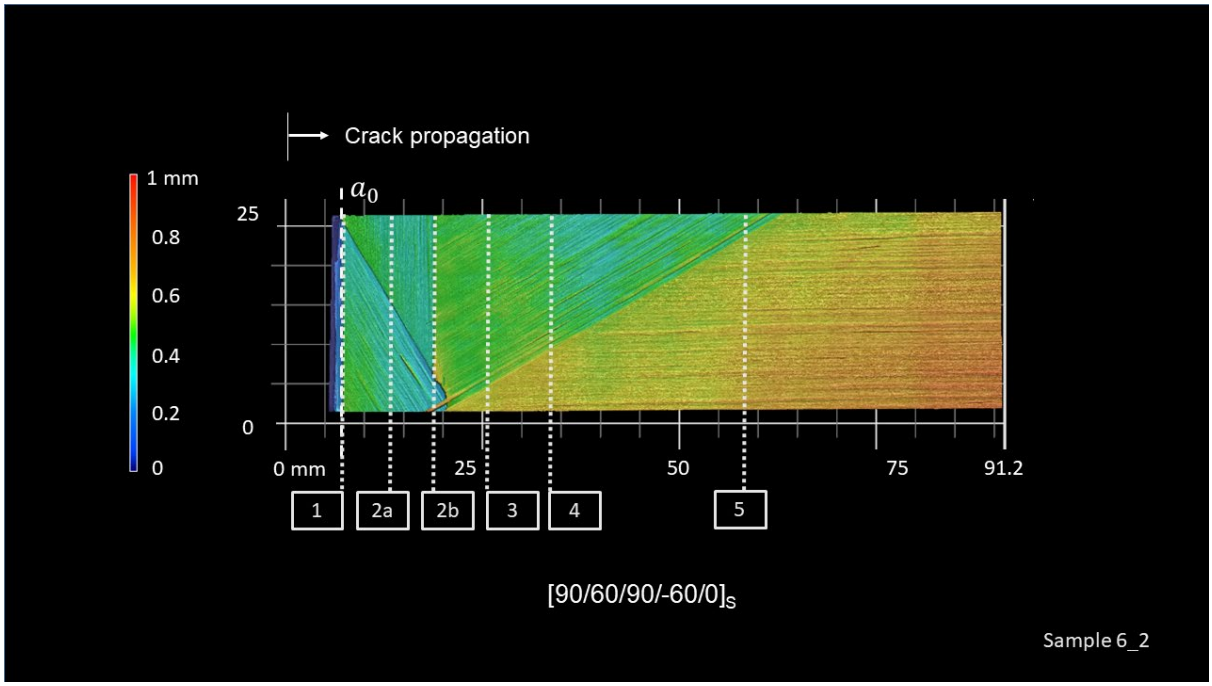

(b)

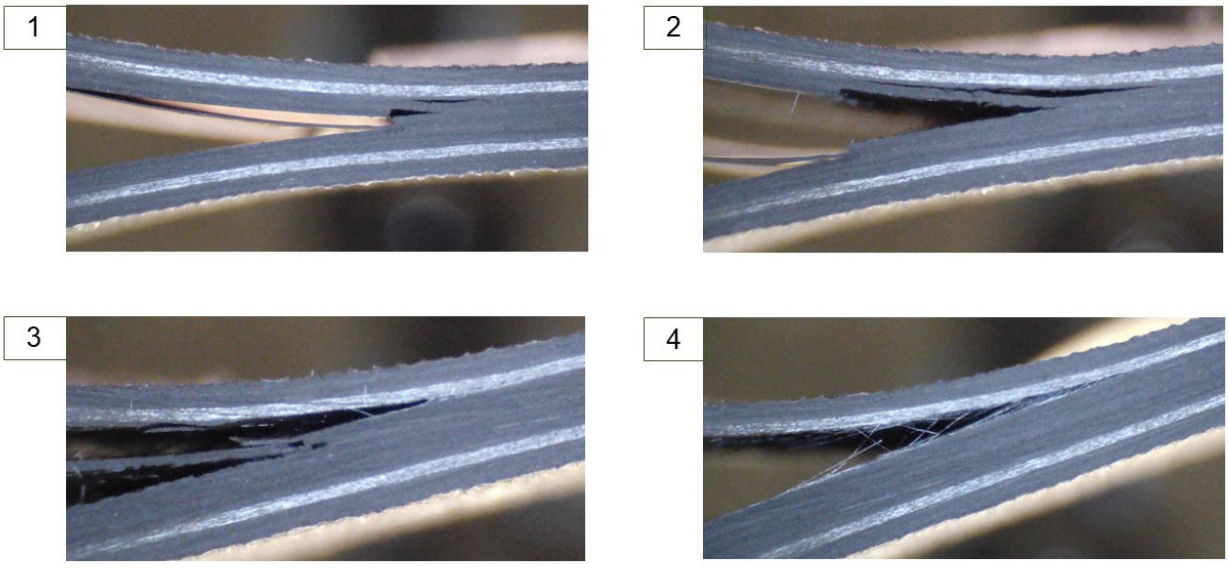

(c)

Figure 15: (a) R-curve, (b) topography and (c) images taken by the travelling microscope of the specimen Araldite_[90/60/90/-60/0]s.

Figure 14 (a) shows an increase in the G_I values between points 1-2 and 3-4. By analysing the fracture surfaces a posteriori (Figure 14 (b), these peaks represent a transition between the

crack propagation paths within the joint. It is also possible to identify a crack deflection between 90 to 45-degree plies (point 2) and transition between 45,-45 and 0-degree plies (close to point 4), followed by a decrease representing the crack deflection to the 0-degree ply and final delamination (almost constant G_I values) in point 5. A similar trend was also observed in the $[90/60/90/-60/0]_S$ specimens, with the peaks in points 2 and 4 that represent the transition regions between multiple fracture surfaces, in particular to 60 to 90 and -60 in point 2 and from -60 to 0 degree.

From images of the travelling microscope (mainly in Figures 14 (c), details 3 and 4, and 15 (b), details 2 and 3), conversely to the other stacking sequences, the crack propagated simultaneously in different plies. This phenomenon is probably driven by the specimens twisting due to the asymmetry promoted in the specimens' adherends since the crack keeps propagating through the composite's thickness [27], [41]. As stated by Khan [29] and Kupski [11], [37], in joints with higher fibre orientation angles next to the adhesive layer, the crack tends to propagate further inside the composite due to increased peel stresses in the layups neighbouring.

Moreover, Figures 14 (b) and 15 (b) confirm that the crack propagated simultaneously in different plies at various crack positions. In Figure 14 (b) at point 3 (between 20 and 25 mm), the crack propagated in both + and -45° plies (confirmed by the different colours graduation, meaning different planes within the joint), staying stable only when the 0° degree ply was reached. Similar behaviour can also be observed in the Araldite_$[90/60/90/-60/0]_S$ specimen, where a crack deflection from the 60°, 90° and -60° plies could be observed within the first 25 mm of propagation.

Figure 16 shows the CZE stiffness degradation in the FEA of AF 163-2k_[90/45/-45/0]s and Araldite_[90/45/-45/0]s.

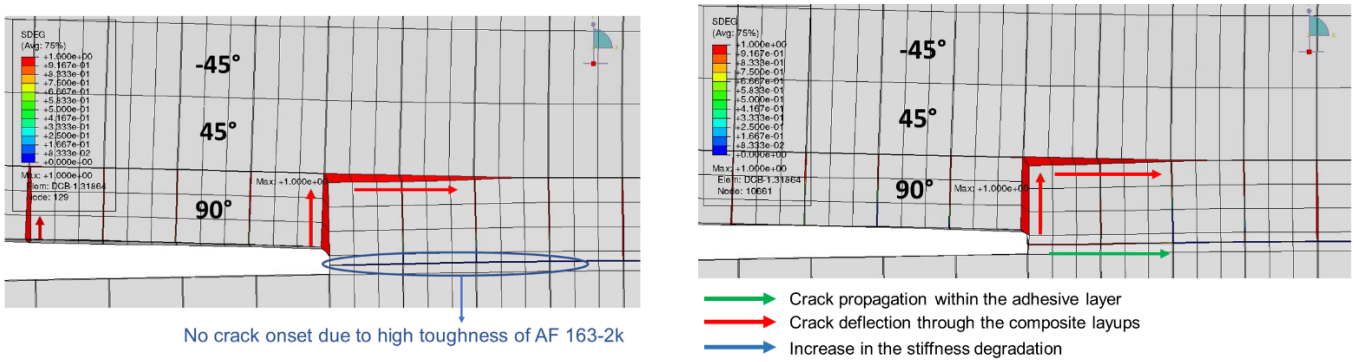

(a) AF 163-2k_[90/45/-45/0]s (b) Araldite_[90/45/-45/0]s

Figure 16: CZE stiffness degradation for (a) AF163-2k_[90/45/-45/0]s and (b) Araldite_ [90/45/-45/0]s.

In Figure 16 (a) of the AF163-2k_[90/45/-45/0]$_S$ specimens, no stiffness degradation was identified in the bondline, indicating that the local stresses that occur in the composite plies overcome the required stresses for fracture onset in the composite plies [30], propagating directly into the composite mid-plane instead of in the bondline. A similar figure is observed for the Araldite_[90/45/-45/0]$_S$, however since we are in presence of a less tough adhesive, it is also possible to see stiffness degradation at the CZE of the bondline and a preferential path for crack onset also within the bondline.

For the 60-degree laminates bonded with both adhesives, the adhesive type did not influence their damage mechanisms since the crack propagation occurred directly within the composite plies. Therefore, for these laminates, the geometric singularities created by the laminate stacking sequence represent a more decisive influence on the joint's fracture mechanisms than the crack tip.

It was observed that once a matrix cracking occurs, it can keep propagating through the composite thickness or in the present interface (delamination), depending on the fibre orientation of the following layup. As also observed in previous works in the literature [11], [27], [29], [37], [42], [43], when the following layup after a matrix cracking has a 0-degree orientation, small stresses singularities are present in a way that the more energetically favourable path for the crack propagates is the delamination at this interface.

Therefore, for the layups with 45 and 60-degree plies orientation, the crack mainly propagated through delamination simultaneously in different layers and multi-cracks that propagated

through the composite's mid-plane until reaching the 0-degree ply, where the crack deflection stopped, and the crack stayed in the 0-degree delamination, as also observed in [42].

In conclusion, CFRP layup tailoring, combined with certain adhesive's mechanical properties, makes it possible to "play" with the geometric singularities within the joints and architect the fracture phenomena in the adhesive joint. Triggering crack competition mechanisms and multiple crack propagation through the composite's mid-plane can increase the joint's resistance against the crack onset. It is a possible direction to delay crack propagation further.

6 Conclusions

The effects of the CFRP layup on the crack propagation of adhesively bonded joints were studied. The possibility of enhancing the joint's fracture toughness through tailored CFRP layup was explored. Based on the results, the following conclusions can be drawn:

- CFRP adhesively bonded joints present complex failure mechanisms mainly triggered by crack deflections and crack competition between different crack locations. These fracture phenomena are influenced by the plies orientations and the stress singularities in the neighbours of the pre-crack tip;
- The fibre orientation of the first plies close to the bondline (interface plies) is crucial for the damage evolution within the bonded joints. 0-degrees interface plies tend to prevent the crack deflection to the composite substrate since the adherents presented high stiffness compared to the other specimens. With the increase of the interface ply angle, the crack tends to propagate through the composite's mid-plane until reaching the next 0 degrees ply, in which the crack propagates rapidly by complete delamination;
- Toughening mechanisms of crack deflection and crack competition observed in AF163-2k_[0/90_2/0]s enhance the fracture toughness at the crack onset by 15%. The triggering of these toughening mechanisms at the crack onset can only be achieved if the toughness of the adhesive is high enough such that the cohesive failure is not the preferred crack path.
- The layups with multi-fibre orientation angles (45°, 60° and 90°) triggered an increase in the joint's R-curve every time a crack deflected to a different ply. In the case of the low-toughness adhesive, the resulting fracture toughness of the joint surpassed the

adhesive toughness, showing a promising solution to enhance the joint's resistance against crack propagation even after crack initiation and possibly delay crack growth.

As a summary, three toughening mechanisms could be achieved by architecting the composite substrates layup:

- At crack onset: substrates with cross-ply laminates in combination with high-toughness adhesives trigger crack competition resulting in an increase of 15% at the crack onset compared with pure cohesive failure.
- During crack propagation: 0 degrees substrates in combination with adhesives with embedded meshes trigger cohesive failure with carrier bridging, resulting in an increase of 24 J/m^2 at each 1 mm increment of the crack.
- At the crack onset and during crack propagations: multidirectional laminates in combination with low-toughness adhesive trigger crack deflections within the laminate that has the potential to surpass the adhesive toughness, resulting in an increase of 30% and 97% of fracture toughness of the Araldite_$[90/45/-45/0]_S$ and Araldite_$[90/60/90/-60/0]_S$ joints respectibely when compared to pure cohesive failure.

Acknowledgements

This article is based upon work from COST Action CA18120 (CERTBOND - https://certbond.eu/), supported by COST (European Cooperation in Science and Technology).

The authors would like to acknowledge the support for the experimental and numerical analysis of the Master's students: Nicholas Rox and Akshit Oswal, from the ENSTA Bretagne.

References

[1] A. C. Marques , A. Mocanu, N. Z. Tomić, S. Balos, E. Stammen, A. Lundevall, S. T. Abrahami, R. Günther, J. M. M. de Kok and S. T. de Freitas, "Review on adhesives and surface treatments for structural applications: Recent developments on sustainability and implementation for metal and composite substrates," *Materials*, vol. 13, no. 24, pp. 1–43, 2020, doi: 10.3390/ma13245590.

[2] M. D. Banea and L. F. M. da Silva, “Adhesively bonded joints in composite materials: An overview,” *Proceedings of the Institution of Mechanical Engineers, Part L: Journal of Materials: Design and Applications*, vol. 223, no. 1, pp. 1–18, 2009, doi: 10.1243/14644207JMDA219.

[3] R. Tao, X. Li, A. Yudhanto, M. Alfano, and G. Lubineau, “Laser-based interfacial patterning enables toughening of CFRP/epoxy joints through bridging of adhesive ligaments,” *Compos Part A Appl Sci Manuf*, vol. 139, no. September, p. 106094, 2020, doi: 10.1016/j.compositesa.2020.106094.

[4] G. Jeevi, S. Kumar Nayak, and M. Abdul Kader, “Review on adhesive joints and their application in hybrid composite structures,” *J Adhes Sci Technol*, vol. 33, pp. 1497–1520, 2019, doi: 10.1080/01694243.2018.1543528.

[5] K. Tserpes, A. Barroso-Caro, P. A. Carraro, V. C. Beber, I. Floros, W. Gamon, M. Kozłowski, F. Santandrea, M. Shahverdi, D. Skejić, C. Bedon and V. Rajčić , “A review on failure theories and simulation models for adhesive joints,” *Journal of Adhesion*, vol. 00, no. 00, pp. 1–61, 2021, doi: 10.1080/00218464.2021.1941903.

[6] G. Viana, M. Costa, M. D. Banea, and L. F. M. da Silva, “A review on the temperature and moisture degradation of adhesive joints,” *Proceedings of the Institution of Mechanical Engineers, Part L: Journal of Materials: Design and Applications*, vol. 231, no. 5, pp. 488–501, 2017, doi: 10.1177/1464420716671503.

[7] M. Kadlec, R. Růžek, and P. Bělský, “Concurrent use of Z-pins for crack arrest and structural health monitoring in adhesive-bonded composite lap joints,” *Compos Sci Technol*, vol. 188, no. December 2019, 2020, doi: 10.1016/j.compscitech.2019.107967.

[8] A. Ruairidh, C. Supervisors, M. G. Droubi, N. Haque, and F. August, “Defect Detection and Condition Assessment of Adhesively-Bonded Joints Using Acoustic Emission,” no. August, 2021.

[9] K. Heller, L. J. Jacobs, and J. Qu, “Characterisation of adhesive bond properties using Lamb waves,” *NDT and E International*, vol. 33, no. 8, pp. 555–563, 2000, doi: 10.1016/S0963-8695(00)00022-0.

[10] S. K. Dwivedi, M. Vishwakarma, and P. A. Soni, “Advances and Researches on Non Destructive Testing: A Review,” *Mater Today Proc*, vol. 5, no. 2, pp. 3690–3698, 2018, doi: 10.1016/j.matpr.2017.11.620.

[11] J. Kupski, D. Zarouchas, and S. Teixeira de Freitas, “Thin-plies in adhesively bonded carbon fiber reinforced polymers,” *Compos B Eng*, vol. 184, p. 107627, 2020, doi: 10.1016/j.compositesb.2019.107627.

[12] S. Daynes and P. M. Weaver, “Stiffness tailoring using prestress in adaptive composite structures,” 2013, doi: 10.1016/j.compstruct.2013.05.059.

[13] D. Eisenhut, N. Moebs, E. Windels, D. Bergmann, I. Geiß, R. Reis and A. Strohmayer., “Aircraft Requirements for Sustainable Regional Aviation,” 2021, doi: 10.3390/aerospace8030061.

[14] R. Tao, X. Li, A. Yudhanto, M. Alfano, and G. Lubineau, “On controlling interfacial heterogeneity to trigger bridging in secondary bonded composite joints: An efficient strategy to introduce crack-arrest features,” *Compos Sci Technol*, vol. 188, no. December 2019, p. 107964, 2020, doi: 10.1016/j.compscitech.2019.107964.

[15] A. Wagih, R. Tao, A. Yudhanto, and G. Lubineau, “Improving mode II fracture toughness of secondary bonded joints using laser patterning of adherends,” *Compos Part A Appl Sci Manuf*, vol. 134, no. April, p. 105892, 2020, doi: 10.1016/j.compositesa.2020.105892.

[16] S. Teixeira de Freitas, D. Zarouchas, and J. A. Poulis, “The use of acoustic emission and composite peel tests to detect weak adhesion in composite structures,” *Journal of Adhesion*, vol. 94, no. 9, pp. 743–766, 2018, doi: 10.1080/00218464.2017.1396975.

[17] A. Güemes, A. Renato Pozo-Morales, A. Fernandez-Lopez, X. F. Sánchez-Romate, M. Sánchez, and A. Ureña, “Strain and damage sensing by CNT modified adhesive films and fiber optic distributed sensing. Comparison of performances in a double lap bonded joint,” pp. 1–6, 2019, [Online]. Available: http://www.ndt.net/?id=25035

[18] S. H. Yoon and D. G. Lee, “In situ crack propagation monitoring in tubular adhesive joints containing quartz nano-particles,” *J Adhes Sci Technol*, vol. 25, no. 16, pp. 1973–1985, 2011, doi: 10.1163/016942410X544776.

[19] A. J. Kinloch, J. H. Lee, A. C. Taylor, S. Sprenger, C. Eger, and D. Egan, “The Journal of Adhesion Toughening structural adhesives via nano-and micro-phase inclusions,” 2010, doi: 10.1080/00218460309551.

[20] D. Quan, N. Murphy, and A. Ivankovic, “Fracture behaviour of a rubber nano-modified structural epoxy adhesive: Bond gap effects and fracture damage zone,” *Int J Adhes Adhes*, vol. 77, no. May, pp. 138–150, 2017, doi: 10.1016/j.ijadhadh.2017.05.001.

[21] Q. Rao, Z. Ouyang, and X. Peng, “Enhancing mode I fracture toughness of adhesively bonded unidirectional composite joints using surfactant-stabilised multi-walled carbon nanotube and graphene nanoplate,” *Polym Test*, vol. 96, Apr. 2021, doi: 10.1016/J.POLYMERTESTING.2021.107110.

[22] A. Buchman, H. Dodiuk-Kenig, A. Dotan, R. Tenne, and S. Kenig, “Toughening of Epoxy Adhesives by Nanoparticles,” *J Adhes Sci Technol*, vol. 23, no. 5, pp. 753–768, 2009, doi: 10.1163/156856108X379209.

[23] R. J. C. Carbas, L. F. M. da Silva, and L. F. S. Andrés, “Functionally graded adhesive joints by graded mixing of nanoparticles,” *Int J Adhes Adhes*, vol. 76, pp. 30–37, Jul. 2017, doi: 10.1016/J.IJADHADH.2017.02.004.

[24] D. Quan, N. Murphy, S. Flynn, M. Artuso, C. Rouge, and A. Ivankovi´civankovi´c, “Interlaminar fracture toughness of CFRPs interleaved with stainless steel fibres Combining deep learning with computational continuum mechanics (SmartSim) View project Surrogate Lung View project Interlaminar fracture toughness of CFRPs interleaved with stainless steel fibres”, doi: 10.1016/j.compstruct.2018.11.016.

[25] S. Minakuchi and N. Takeda, “Arresting crack in composite bonded joint under fatigue using fiber-reinforcement-based feature,” *International SAMPE Technical Conference*, no. August, pp. 199–206, 2017.

[26] C. Bach, R. Jebari, A. Viti, and R. Hewson, “Composite stacking sequence optimisation for aeroelastically tailored forward-swept wings,” *Structural and Multidisciplinary Optimisation*, vol. 55, no. 1, pp. 105–119, Jan. 2017, doi: 10.1007/S00158-016-1477-3/METRICS.

[27] B. D. Davidson, R. Krüger, and M. König, “Effect of stacking sequence on energy release rate distributions in multidirectional DCB and ENF specimens,” *Eng Fract Mech*, vol. 55, no. 4, pp. 557–569, 1996, doi: 10.1016/S0013-7944(96)00037-9.

[28] M. Frascio, E. A. S. Marques, R. J. C. Carbas, L. F. M. Da Silva, M. Monti and M. Avalle , “Review of Tailoring Methods for Joints with Additively Manufactured Adherends and Adhesives”, doi: 10.3390/ma13183949.

[29] M. A. Khan, “Development of rules for the design of adhesively bonded fibre-reinforced plastic composite joints in aerospace applications,” 2018.

[30] R. Lopes Fernandes, S. Teixeira de Freitas, M. K. Budzik, J. A. Poulis, and R. Benedictus, “From thin to extra-thick adhesive layer thicknesses: Fracture of bonded joints under mode I loading conditions,” *Eng Fract Mech*, vol. 218, Sep. 2019, doi: 10.1016/J.ENGFRACMECH.2019.106607.

[31] J. Kupski, S. Teixeira de Freitas, D. Zarouchas, P. P. Camanho, and R. Benedictus, “Composite layup effect on the failure mechanism of single lap bonded joints,” *Compos Struct*, vol. 217, pp. 14–26, Jun. 2019, doi: 10.1016/J.COMPSTRUCT.2019.02.093.

[32] A. Ozel, B. Yazici, S. Akpinar, M. D. Aydin, and Ş. Temiz, “A study on the strength of adhesively bonded joints with different adherends,” *Compos B Eng*, vol. 62, pp. 167–174, Jun. 2014, doi: 10.1016/J.COMPOSITESB.2014.03.001.

[33] L. A. Burns, A. P. Mouritz, D. Pook, and S. Feih, “Strength improvement to composite T-joints under bending through bio-inspired design,” *Compos Part A Appl Sci Manuf*, vol. 43, no. 11, pp. 1971–1980, Nov. 2012, doi: 10.1016/J.COMPOSITESA.2012.06.017.

[34] “HexPly ® 8552 Epoxy matrix (180°C/356°F curing matrix),” 2020.

[35] “Standard Test Method for Mode I Interlaminar Fracture Toughness of Unidirectional Fiber-Reinforced Polymer Matrix Composites.” https://www.astm.org/d5528-13.html (accessed Sep. 10, 2022).

[36] A. Turon, J. Costa, P. P. Camanho, and C. G. Dávila, “Simulation of delamination in composites under high-cycle fatigue,” *Compos Part A Appl Sci Manuf*, vol. 38, no. 11, pp. 2270–2282, 2007, doi: 10.1016/j.compositesa.2006.11.009.

[37] J. Kupski, S. Teixeira de Freitas, D. Zarouchas, P. P. Camanho, and R. Benedictus, “Composite layup effect on the failure mechanism of single lap bonded joints,” *Compos Struct*, vol. 217, pp. 14–26, Jun. 2019, doi: 10.1016/J.COMPSTRUCT.2019.02.093.

[38] “Araldite ® 2015-1 Two component epoxy paste adhesive Key properties”, Accessed: Sep. 10, 2022. [Online]. Available: www.aralditeadhesives.com.

[39] Nicolas P. Lavalette, Otto K. Bergsma, Dimitrios Zarouchas, Rinze Benedictus, Influence of geometrical parameters on the strength of Hybrid CFRP-aluminium tubular adhesive joints, Composite Structures, Vol. 240, 2020, https://doi.org/10.1016/j.compstruct.2020.112077.

[40] Moroni, F.; Pirondi, A.; Pernechele, C.; Vescovi, L. Comparison of Tensile Strength and Fracture Toughness of Co-Bonded and Cold-Bonded Carbon Fiber Laminate-Aluminum Adhesive Joints. *Materials* 2021, *14*, 3778. https://doi.org/10.3390/ma14143778

[41] M. F. Abd Rased and S. H. Yoon, “Experimental study on effects of asymmetrical stacking sequence on carbon fiber/epoxy filament wound specimens in DCB, ENF, and MMB tests,” *Composite Structures*, vol. 264. 2021. doi: 10.1016/j.compstruct.2021.113749.

[42] M. D. Aydin, “3-D Nonlinear Stress Analysis on Adhesively Bonded Single Lap Composite Joints with Different Ply Stacking Sequences,” *http://dx.doi.org/10.1080/00218460801888359*, vol. 84, no. 1, pp. 15–36, Jan. 2008, doi: 10.1080/00218460801888359.

[43] S. Purimpat, R. Jérôme, and A. Shahram, “Effect of fiber angle orientation on a laminated composite single-lap adhesive joint,” *http://dx.doi.org/10.1080/09243046.2013.782805*, vol. 22, no. 3, pp. 139–149, Jun. 2013, doi: 10.1080/09243046.2013.782805.